Langmuir
Article
pubs.acs.org/Langmuir

On the Breakup of Patterned Nanoscale Copper Rings into Droplets via Pulsed-Laser-Induced Dewetting: Competing Liquid-Phase Instability and Transport Mechanisms

Yueying Wu,[†] Jason D. Fowlkes,[‡] Philip D. Rack,*[,†,‡] Javier A. Diez,[∥] and Lou Kondic[§]

[†]*Department of Materials Science and Engineering, The University of Tennessee, Knoxville, Tennessee 37996,* [‡]*The Oak Ridge National Laboratory, Oak Ridge, Tennessee 37831,* [∥]*Instituto de Física Arroyo Seco, Universidad Nacional del Centro de la Provincia de Buenos Aires (UNCPBA), Pinto 399, Tandil, Argentina, and* [§]*Department of Mathematical Sciences, Center for Applied Mathematics and Statistics, New Jersey Institute of Technology, Newark, New Jersey*

Received April 7, 2010. Revised Manuscript Received June 9, 2010

Nanolithographically patterned copper rings were synthesized, and the self-assembly of the rings into ordered nanoparticle/nanodrop arrays was accomplished via nanosecond pulsed laser heating above the melt threshold. The resultant length scale was correlated to the transport and instability growths that occur during the liquid lifetime of the melted copper rings. For 13-nm-thick rings, a change in the nanoparticle spacing with the ring width is attributed to a transition from a Raleigh−Plateau instability to a thin film instability because of competition between the cumulative transport and instability timescales. To explore the competition between instability mechanisms further, we carried out experiments with 7-nm-thick rings. In agreement with the theoretical predictions, these rings break up in both the azimuthal and radial directions, confirming that a simple hydrodynamic model captures the main features of the processes leading to the breakup.

Introduction

Wetting and dewetting phenomenon have long been studied because they are critical to understanding many fluid dynamics and transport phenomena. Although fluid transport and dewetting phenomenon have been studied on multiple length scales, interesting transport (for a recent review, see ref 1) and instability (for a recent review, see ref 2) mechanisms and regimes emerge at nanometer length scales. Although many studies have investigated the transport[3−5] and instability of polymeric thin films[6,7] and rivulets,[8−11] the breakup of thin metal films in the solid and liquid states is of interest because of their different physical and chemical properties.[12−14] In the liquid state, the metal viscosity is much lower and the surface energy is much higher relative to those of many polymers. The interaction between a metal and the substrate is characterized by an additional long-range interaction due to the kinetic energy of free electrons in the metal, as put forward some time ago[15] and reviewed recently.[16] This interaction can be included via a disjoining pressure model, which has been extensively used to model the liquid−solid interaction in thin films.[2,13] Although a variety of models exist, it is of interest to determine whether a simple model discussed later in this work can be used to explain the main features of the experiments involving liquid-metal instabilities. This motivation has in part driven recent renewed interest in pulsed laser heating of metal thin films and the associated instabilities and transport that leads to correlated nanodrop size and spacing.[17−20] We have shown that nanoscale-patterned nickel lines[21] and other geometries[22] experience competing instability mechanisms because of surface perturbations and edge effects related to the finite length of the metal lines liquefied by pulsed laser heating. The experimental time and length scales for the edge and Rayleigh−Plateau instability were surprisingly adequately reproduced by employing a numerical method using the long-wave approximation of the Navier−Stokes equations. To follow up on this initial study, here we present results using nanometer-scale patterned metal (copper) rings. Rings are intriguing structures for investigating instabilities that lead to liquid film breakup and droplet formation, in view of

*To whom correspondence should be addressed. E-mail: prack@utk.edu.

(1) Bonn, D.; Eggers, J.; Indekeu, J.; Meunier, J.; Rolley, E. *Rev. Mod. Phys.* **2009**, *81*, 739.
(2) Craster, R. V.; Matar, O. K. *Rev. Mod. Phys.* **2009**, *81*, 1131.
(3) Jacobs, K.; Seemann, R.; Schatz, G.; Herminghaus, S. *Langmuir* **1998**, *14*, 4961.
(4) Redon, C.; Brochard-Wyart, F.; Rondelez, F. *Phys. Rev. Lett.* **1991**, *66*, 715.
(5) Thiele, U.; Mertig, M.; Pompe, W. *Phys. Rev. Lett.* **1998**, *80*, 2869.
(6) Becker, J.; Grün, G.; Seemann, R.; Mantz, H.; Jacobs, K.; Mecke, K. R.; Blossey, R. *Nat. Mat.* **2003**, *2*, 59.
(7) Reiter, G.; Sharma, A.; Casoli, A.; David, M.-O.; Khanna, R.; Auroy, P. *Langmuir* **1999**, *15*, 2551.
(8) Diez, J.; Kondic, L. *Phys. Fluids* **2007**, *19*, 072107.
(9) Callegari, G.; Calvo, A.; Hulin, J. P.; Brochard-Wyart, F. *Langmuir* **2002**, *18*, 4795.
(10) McCallum, M. S.; Voorhees, P. W.; Miksis, M. J.; Davis, S. H.; Wong, H. *J. Appl. Phys.* **2002**, *79*, 7604.
(11) Brochard-Wyart, F.; Redon, C. *Langmuir* **1992**, *8*, 2324.
(12) Bischof, J.; Scherer, D.; Herminghaus, S.; Leiderer, P. *Phys. Rev. Lett.* **1996**, *77*, 1536.
(13) Herminghaus, S.; Jacobs, K.; Mecke, K.; Bischof, J.; Fery, A.; Ibn-Elhaj, M.; Schlagowski, S. *Science* **1998**, *282*, 916.
(14) Habenicht, A.; Olapinski, M.; Burmeister, F.; Leiderer, P.; Boneberg, J. *Science* **2005**, *309*, 2043.
(15) Derjaguin, B. V.; Leonov, L. F.; Roldughin, V. I. *Colloid Interface Sci.* **1985**, *108*, 107.
(16) Ajaev, V.; Willis, D. *Phys. Fluids* **2003**, *15*, 3144.
(17) Trice, J.; Thomas, D.; Favazza, C.; Sureshkumar, R.; Kalyanaraman, R. *Phys. Rev. B* **2007**, *75*, 235439.
(18) Trice, J.; Favazza, C.; Thomas, D.; Garcia, H.; Kalyanaramn, R.; Sureshkumar, R. *Phys. Rev. Lett.* **2008**, *101*, 017802.
(19) Favazza, C.; Kalyanaraman, R.; Sureshkumar, R. *Nanotechnology* **2006**, *17*, 4229.
(20) Krishna, H.; Shirato, N.; Favazza, C.; Kalyanaraman, R. *Phys. Chem.* **2009**, *11*, 8136.
(21) Kondic, L.; Diez, J.; Rack, P.; Guan, Y.; Fowlkes, J. *Phys. Rev. E* **2009**, *79*, 026302.
(22) Rack, P.; Guan, Y.; Fowlkes, J.; Melechko, A.; Simpson, M. *Appl. Phys. Lett.* **2008**, *92*, 223108.

the fact that this geometry eliminates edge effects. To simplify this study, large-radius rings were studied so as to minimize additional Laplace pressures associated with the azimuthal curvature.

Our previous studies have focused on the breakup and assembly of thin metal films[23,24] for the subsequent catalytic growth of 1D carbon nanofibers[25] for a variety of nanoscale applications. (See refs 26 and 27 for reviews.) The ability to direct the assembly of metallic nanostructures with correlated size and length scales has far-reaching possibilities from organized nanomagnetics and plasmonics to functional biological assays. Thus with these applications in mind and the goal of understanding general principles of self-assembly, we study the fundamental length scales and timescales associated with the pulsed-laser-induced dewetting of copper rings into correlated nanodrops.

Experiment

In this study, we investigate the liquid-phase breakup of nanoscale copper rings heated via pulsed laser exposure above the melt threshold. Initially, twenty 5-μm-radius and twenty 10-μm-radius copper rings (sufficient for the Laplace pressure due to azimuthal curvature to be negligible) with various ring widths were patterned onto (100)-oriented single-crystal silicon substrates. No attempt to remove the native oxide was made. Each ring was electron beam patterned into a positive-tone thin poly(methyl methacrolate) (PMMA) film. A 13 nm copper film was subsequently sputter deposited, and the ring pattern was realized by dissolving or lifting off the original PMMA film in an acetone bath for ~1 h. The ring widths ranged from 93 to 441 nm as measured by scanning electron microscopy. Subsequently, a KrF 25 ns pulsed laser at a 248 nm wavelength was used to expose all of the ring patterns simultaneously to 10 laser pulses at a fluence of 420 mJ/cm^2, which is sufficient to melt the copper film and ultimately form an array of ordered nanodrops. For future reference, we note that simple simulations of heat transport across a 13-nm-thick film have shown that laser heating leads to a 60 ns liquid lifetime per pulse.[28] Figure 1a shows electron micrographs of five different 5-μm-radius rings with different widths after laser exposure, which demonstrates the resultant nanoparticles after 10 laser pulses. Figure 1b is a plot of the average particle spacing versus the measured ring width for the two ring diameters. Although the focus of this study compares the average spacing, consistent with the instability mechanisms described below, a typical distribution of particle spacings (and consequently particle size) is illustrated by the histogram insets to Figure 1b for 110-nm-wide rings of 5 μm radius.

Subsequent to synthesizing and pulse laser dewetting the 13 nm copper, a set of 7 nm copper rings were also synthesized using the same procedure. For later reference, we note that there is some metal mass loss taking place during laser irradiation, possibly as a result of evaporation and diffusion into the substrate. We estimate this loss to be in the range of 5−10% per laser pulse.

Our initial expectation for the laser-treated rings was that we would see a monotonic increase in the nanodrop spacing with ring width, consistent with the contraction of rings to semicylindrical strips and the subsequent breakup due to a Rayleigh−Plateau-type of instability, modified by the presence of the substrate.[9−11,21] This expectation is consistent with recent observations by McGraw et al.,[29] who showed that for polystyrene toroids the number of Rayleigh−Plateau instability wavelengths scaled with the ratio of the toroid radius/width. However, in their case, they also observed radial transport associated with the azimuthal curvature, which as described above we do not observe here. Figure 1b, however, shows an interesting trend in the nanodrop spacing for the combined 5- and 10-μm-radius rings as a function of the measured ring width. There is an increase in the nanodrop spacing with increasing ring width up to approximately 200 nm, where there appears to be a discontinuity/shift to a lower and almost constant particle spacing. Despite the relatively large scatter in the results, this puzzling transition at close to 200 nm is obvious and requires explanation.

Model

To gain a better understanding of the breakup process, similar to our previous work,[21] we realize that the transport and instability growth during the liquid lifetime dominates the solid-state transport (see also refs 17 and 30 regarding this point), and we concentrate on modeling a Newtonian liquid film. We furthermore use the fact that the 25 ns pulsed laser irradiation allows for very rapid heating to assume that all thermal related effects take place on a timescale that is much shorter than the timescale on which the evolution takes place so that we may consider a film at fixed temperature. Finally, we apply a long-wave (lubrication) approximation, allowing us to reduce the otherwise very complicated problem to a tractable formulation. The issues and necessary approximations involved in applying the lubrication approach to a problem characterized by relatively large contact angles are discussed elsewhere.[21,31] Within this approach, the following single nonlinear fourth-order partial differential equation governs the evolution,[8]

$$3\mu\frac{\partial h}{\partial t}+\gamma\nabla\cdot(h^3\nabla\nabla^2 h)+\nabla\cdot[h^3\nabla\Pi(h)]=0 \qquad (1)$$

where $h(x, y, t)$ is the film thickness, x and y are the in-plane coordinates, $\nabla=(\partial/\partial x, \partial/\partial y)$, μ is the dynamic viscosity, and γ is the surface tension. Here, the second term corresponds to the capillary forces and the third term is due to liquid−solid interaction. The disjoining pressure, $\prod(h)$, is related by differentiation to the interfacial potential, $\varphi(h)$. The functional form of $\prod(h)$, which we have used in our recent work,[8,21,31] is of a form corresponding to an interface potential that has competing long- and short-range forces and has a minimum at nanoscale lengths,[32]

$$\Pi(h)=\kappa f(h)=\kappa\left[\left(\frac{h_*}{h}\right)^n-\left(\frac{h_*}{h}\right)^m\right] \qquad (2)$$

introducing κ (proportional to the Hamaker constant), the equilibrium film thickness, h_* (corresponding to the minimum of the potential $\varphi(h)$[32]), and the exponents $n > m > 1$. The first term represents liquid−solid repulsion, and the second term is attractive, leading to a stable film thickness of $h = h_*$. Within the present context, this second term includes the electronic component of the disjoining pressure,[15,16] which is briefly discussed in the Introduction. Here, $\kappa = S/(Nh_*)$, where S is the spreading parameter, and $N = (n - m)/((m - 1)(n - 1))$. The spreading parameter can be related to the apparent contact angle θ via Laplace−Young condition $S = \gamma(1-\cos\theta)$. In the present work, we use $(n, m) = (3, 2)$;[16] see also Remark 2 below.

(23) Guan, Y. F.; Pearce, R. C.; Melechko, A. V.; Hensley, D. K.; Simpson, M. L.; Rack, P. D. *Nanotechnology* **2008**, *19*, 235604.
(24) Klein, K. L.; Melechko, A. V.; Rack, D. P.; Fowlkes, J. D.; Meyer, H. M.; Simpson, M. L. *Carbon* **2005**, *143*, 1857.
(25) Melechko, A. V.; Merkulov, V. I.; McKnight, T. E.; Guillorn, M. A.; Klein, K. L.; Lowndes, D. H.; Simpson, M. L. *J. Appl. Phys.* **2005**, *97*, 041301.
(26) Klein, K. L.; Melechko, A. V.; McKnight, T. E.; Retterer, S. T.; Rack, P. D.; Fowlkes, J. D.; Joy, D. C.; Simpson, M. L. *J. Appl. Phys.* **2008**, *103*, 061301.
(27) Melechko, A. V.; Desikan, R.; McKnight, T. E.; Klein, K. L.; Rack, P. D. *J. Appl. Phys.* **2009**, *42*, 193001.
(28) Pedraza, A. J.; Guan, Y. F.; Fowlkes, J. D.; Smith, D. A. *J. Vac. Sci. Technol., B* **2004**, *22*, 2823.
(29) McGraw, J. D.; Li, J.; Tran, D. L.; Shi, A.-C.; Dalnoki-Veress, K. *Soft Matter* **2010**, *6*, 1258.
(30) Favazza, C.; Trice, J.; Kalyanaraman, R.; Sureshkumar, R. *Appl. Phys. Lett.* **2007**, *91*, 043105.
(31) Diez, J.; González, A. G.; Kondic, L. *Phys. Fluids* **2009**, *21*, 082105.
(32) Seemann, R.; Herminghaus, S.; Jacobs, K. *Phys. Rev. Lett.* **2001**, *86*, 5534.

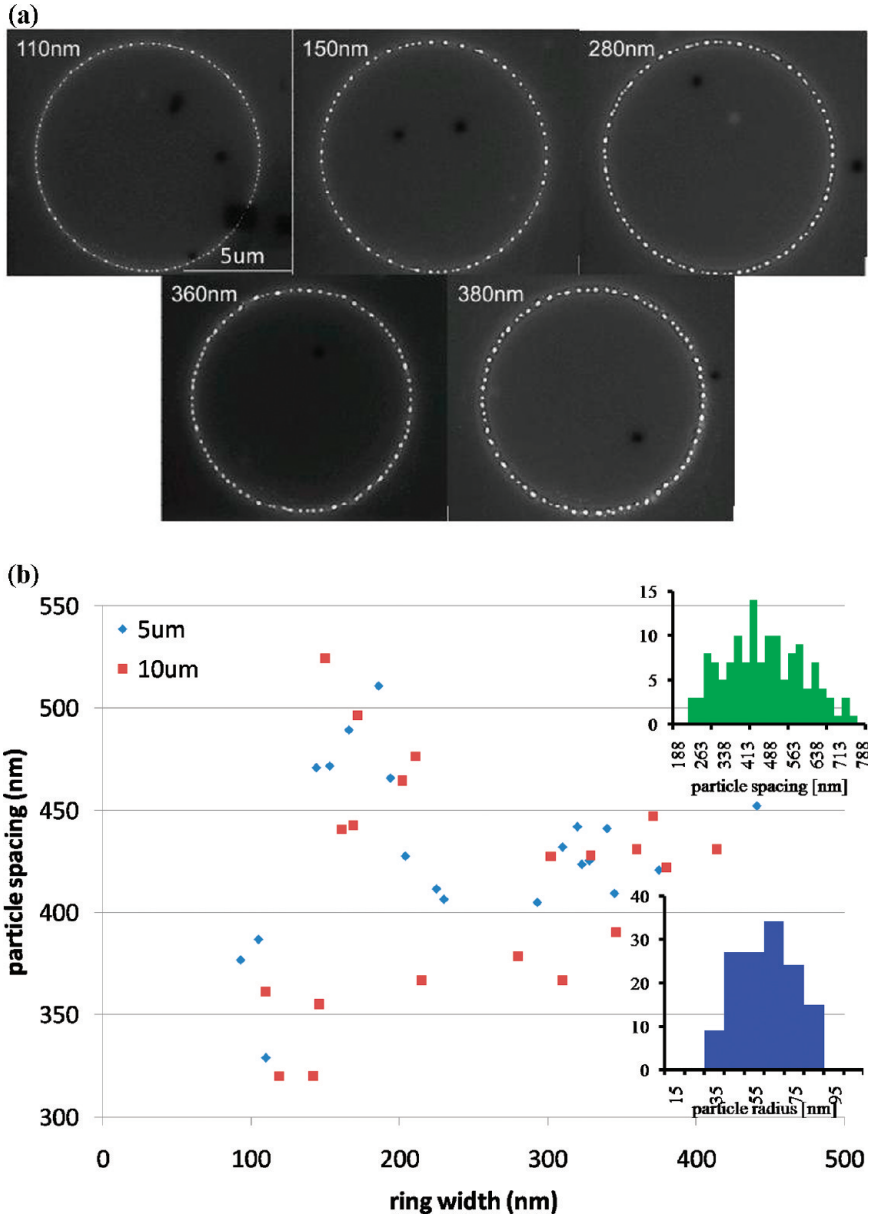

Figure 1. (a) Scanning electron micrographs of the $h_0 = 13$-nm-thick, 5-μm-radius copper rings of variable width after 10 pulses. (b) Plot of average nanodrop spacing for twenty 5-μm-radius and twenty 10-μm-radius rings as a function of the measured widths. Insets show the histograms of the droplet spacing (upper right) and droplet radius (lower right) for 110-nm-wide rings of 5 μm radius. The standard deviation of the typical histogram spacing is 126 nm.

Remark 1. For simplicity, we do not include the presence of the native silicon oxide layer because the measured wetting angle of the resultant copper droplets (~50°) was close to the expected value for copper on silicon (~59°) relative to copper on silicon oxide (~90°). An analysis of the possible influence of the native silicon oxide layer is left for future work.

Remark 2. A justification of the simple version of disjoining pressure used (in particular, for the same coefficients in front of the two terms) can be found in recent work on a related topic.[33] The choice of exponents is less obvious, but we expect that the exact functional form is not crucial. Still, the long-range behavior appears to be dominated by $1/h^2$ behavior.[15] The negative sign of the corresponding term in the dijsoining pressure is consistent (although not required) with the formulation;[15] such a sign has been used in recent work on liquid metals.[13,16] We note that this negative term leads to the existence of a pressure minimum and to the possibility of spinodal dewetting of a thin film, discussed in what follows.[13]

Estimating the Hamaker Constant

Critical to understanding the length scale and timescale associated with the ring instabilities and nanodrop breakup is an estimate of the equilibrium thickness, h_*. This is equivalent to determining the Hamaker constant, $\mathcal{A}$, assuming that these quantities are related by $\mathcal{A} = 6\pi\kappa h_*^3$ (e.g., refs 2 and 33). To estimate $\mathcal{A}$ (or h_*), a thin film of copper was sputter deposited onto silicon. More precisely, a thickness gradient was sputtered across a 100-mm-long strip of silicon.[34] The film thickness was measured via optical reflectometry every 10 mm across the sample (Figure 2). The wafer was diced, and five samples were laser

(33) Gomba, J.; Homsy, G. M. *Langmuir* **2009**, *25*, 5684.

(34) Klein, K. L.; Melechko, A. V.; D.Rack, P.; Fowlkes, J. D.; Meyer, H. M.; Simpson, M. L. *Carbon* **2005**, *43*, 1857.

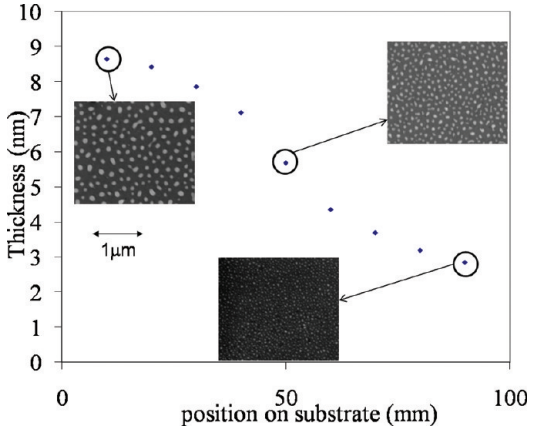

Figure 2. Sputtered copper film thickness as a function of substrate position with insets of scanning electron micrographs of the resultant nanoparticle distributions of three copper film thicknesses after pulse laser treatment.

Table 1. Material Properties Used for Hydrodynamic Simulations and Linear Stability Analysis (LSA) Calculations

copper liquid viscosity	4.38 mPa s
copper liquid density	8 g/cm^3
Cu−Si surface energy	0.076 N/m
Si−air surface energy	0.75 N/m
Cu−air surface energy	1.304 N/m
liquid copper wetting angle	59°

treated with three 420 mJ/cm^2 pulses, sufficient for the film in each sample to dewet and form nanodrops. Subsequently, scanning electron micrographs of the resultant nanodrops were taken (see Figure 2 insets for three example micrographs), and droplet sizes and spacings were determined using an imaging software analysis program and the fast Fourier transform of the image, respectively.

The spacings found experimentally above were related to the predictions of the linear stability analysis (LSA) of the 1D version of eq 1, assuming the functional form of the disjoining pressure given by eq 2. This analysis is carried out in the usual manner, assuming that the infinite film is perturbed by small perturbations, and then finding the most unstable mode.[8] The comparison between the wavelength of this most unstable mode and the experimental spacing then enabled us to extract a Hamaker constant of approximately 1.56×10^{-17} J. We note that this procedure is only approximated because LSA (assuming small perturbations) is used, and the distance between particles is a result of nonlinear evolution; however, it is expected that this approach is reasonably accurate. This value of $\mathcal{A}$ corresponds to the precursor thickness of $h_* \approx 0.81$ nm. Although this is larger than typical van der Waals length scales, it is in reasonable agreement with Bischoff et al.,[12] who investigated the spinodal breakup of gold thin films.[13] They determined a characteristic length scale for the gold/silica system on the order of 2.5×10^{-17} J. Work by Trice et al.[17] using a regression of the droplet spacing versus the square of the thickness (h_0^2) for cobalt resulted in an effective Hamaker coefficient of $\sim 1.4 \times 10^{-18}$ J.

Discussion

With the Hamaker constant relevant to our system known and the film properties listed in Table 1, we proceed to consider the evolution of the ring geometry using the formulation based on the governing equation (eq 1). We note that most of our conclusions will be based on the further use of linear stability analysis, which only approximately describes nonlinear processes responsible for instability and breakup. Therefore, we are not looking

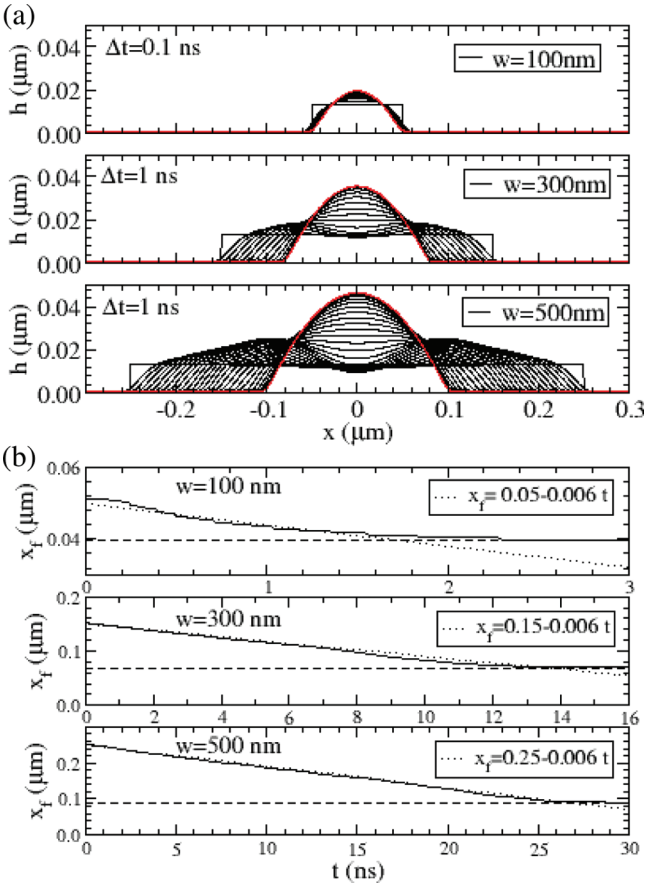

Figure 3. One dimensional time-dependent simulations of the h_0 = 13-nm-thick copper ring cross section for 100-, 300-, and 500-nm-wide rings (ignoring azimuthal curvature). (a) Temporal profiles of the film/strip height of the 100-, 300-, and 500-nm-wide rings demonstrating the timescale for formation of a semicylindrical shape for each ring width. (b) Edge (front) position, x_f, as a function of time. The solid line follows from simulations, and the dotted line is a linear fit as shown.

for exact agreement but hope to understand the main features of the experimental results. In particular, for most of the work, we ignore the azimuthal radius of curvature of a ring. This can be justified by considering the Dean number, D, which is basically the usual Reynolds number $Re = \rho V w/\mu$ multiplied by $(w/2R)^{1/2}$, where V is the azimuthal velocity and R is the radius of the ring. Because we do not observe any important azimuthal flow, it is expected that the azimuthal velocity is much smaller than the radial velocity. Thus, we can make an estimate by considering the worst-case scenario where V is of the same order of magnitude as the radial velocity, which is estimated experimentally to be about 6 m/s. We take w = 500 nm and R = 5 μm and obtain $D \approx 1$. Because the influence of azimuthal curvature is expected only for much larger values of D,[35] we find that for the problem considered here the effects of azimuthal curvature appear not to be important.

First, we consider just a cross section of a strip. Therefore, we concentrate for a moment on a semi-infinite film with variable width comparable to that in experiments and infinite length in the perpendicular direction. Time-dependent simulations of the corresponding 1D version of eq 1 (x is the direction across the ring) were performed to understand the evolution. Figure 3a shows the cross section of the 13-nm-thick film with widths of w = 100, 300, and 500 nm. The 100-nm-wide ring simply redistributes material

(35) Berger, S.; Talbot, L.; Yao, L.-S. *Annu. Rev. Fluid Mech.* **1983**, *15*, 461.

to minimize the surface area. However, the 300- and 500-nm-wide rings contract at a velocity of ~6 m/s until they reach the equilibrium shape (and thus form a semicylindrical strip). Figure 3b shows the edge position as a function of time, revealing the approximate time period required for a strip to form. These times are ~1.7, 13, and 27 ns for the 100-, 300-, and 500-nm-wide rings, respectively.

Now we return to the physical 3D problem of a semi-infinite thin film approximating ring geometry but still ignoring azimuthal curvature. The stability properties of such a film were discussed theoretically in our recent work,[8,31] and here we briefly summarize the results in the present context. First, a flat (infinite) film may be subject to a spinodal type of instability; that is, small surface perturbation may grow and lead to breakup. In addition, a nucleation type of instability may be relevant, as discussed also in the context of liquid metal films (e.g. ref 13). These instability mechanisms are further influenced by the finite film size because the presence of fronts (film edges) contributes to instability development. In this work, we will consider the spinodal-type of instability as representative of thin film instability and defer the discussion of various types of thin film instabilities to future work; in any case, as will become apparent below, what is of relevance here is the scaling of the distance between the droplets with the ring width of w and both spinodal- and nucleation-type instabilities predict that this distance is independent of w. Next, ignoring for a moment film instability mechanisms and assuming that an infinite strip forms as shown in Figure 3, we realize that such a strip is subject to a Rayleigh−Plateau (R-P) type of instability, modified by the presence of the substrate.[21,31] As we discuss next, an interplay of these two instability mechanisms appears to be responsible for the experimental observations.

Considering first the LSA of a thin film of thickness h_0, we find the expression for the wavelength of maximum growth to be[8]

$$\lambda_{m,tf} = 2\pi\left[\frac{\kappa}{2\gamma}\left.\frac{df}{dh}\right|_{h_0}\right]^{-1/2} \quad (3)$$

and the value of the corresponding growth rate to be

$$\sigma_{m,tf} = \frac{16\gamma\pi^4}{3\mu}\frac{{h_0}^3}{{\lambda_{m,tf}}^4} \quad (4)$$

However, when a similar approach is applied to a strip of a given cross section $A = h_0 w$ in equilibrium under capillary and van der Waals forces, we have[31]

$$\lambda_{m,strip} = 2\pi(2A)^{1/2}\left(\frac{M}{1-\cos\theta}\right)^{1/4} \quad (5)$$

with an approximate growth rate of[11,31]

$$\sigma_{m,strip} = \frac{\gamma}{6\mu}F(\theta)A^{-1/2} \quad (6)$$

where

$$F(\theta) = 0.0379\frac{\theta^3}{\sin\theta}\left(\theta - \frac{\sin 2\theta}{2}\right)^{1/2} \quad (7)$$

Figure 4 shows the length scale and timescale for liquid copper on silicon based on the Hamaker constant calculated above and the material properties listed in Table 1 for $(n, m) = (3, 2)$. This Figure also shows averaged experimental data from Figure 1b, with the error bars resulting from the averaging procedure. The averaging procedure for the data presented in Figure 4b involved ordering all of the measured 5 and 10 μm ring widths shown in Figure 1b from smallest to largest and grouping (four to six data points each) the ring widths and resultant spacings; the averages (and appropriate standard deviations) of the grouped ring widths and associated spacings are presented in Figure 4b.

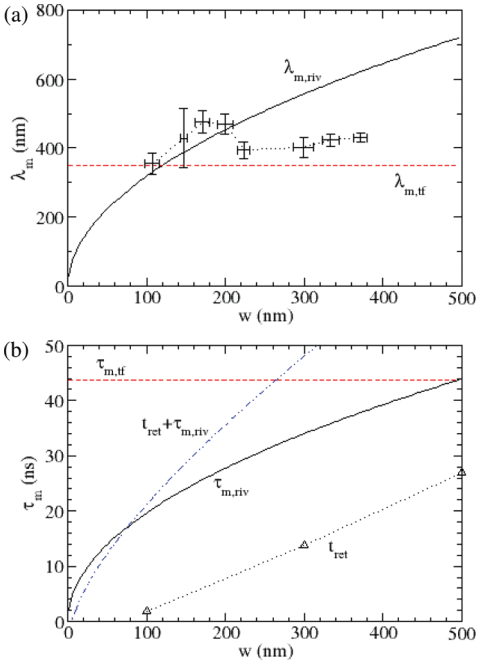

Figure 4. Length scale and timescale from linear stability analysis (LSA) and simulations for the h_0 = 13-nm-thick copper strip as a function of the width, w. (a) Wavelength of the maximum growth rate, λ_m, for the Rayleigh−Plateau (R-P, −, $\lambda_{m,riv}$) and thin film (---, $\lambda_{m,tf}$) instabilities with experimental ring spacings (symbols) included, illustrating the apparent shift in length scale from an R-P to a thin film (spinodal) instability for $w > 200$ nm. (b) Inverse of the maximum growth rate, $\tau_m = 1/\sigma_m$, for the R-P ($\tau_{m,riv}$, −) and thin film (spinodal) ($\tau_{m,tf}$, ---) instabilities. The symbols (···△···) are numerically calculated retraction times, t_{ret}, obtained from Figure 3b. The summation of t_{ret} and $\tau_{m,riv}$ is shown by the dashed−dotted line. All calculations are based on the calculated Hamaker coefficient and the material properties in Table 1.

As demonstrated in Figure 4b, the distance between the droplets that form for rings of up to ~200 nm wide appears to follow the length scale expected from the R-P instability mechanism. The wider rings were expected to follow this behavior as well, leading to a progressively larger spacing proportional to the square root of the ring width, w (eq 5). However, the length scale associated with the distance between the particles that form as a result of the breakup of these wider rings appears to shift to a shorter one. The new instability length scale is almost constant as a function of w, as expected from the spinodal instability mechanism; see eq 3.

Remark 1. We note that, strictly speaking, LSA predicts only a typical value of the distance between the droplets, which is expected to be close to the wavelength of maximum growth. However, the distribution of unstable wavelengths is rather broad; therefore, it is not surprising to find a range of values, as found in the experiments; see Figure 1.

Remark 2. We note that Trice et al.[19] also observed a significant discontinuity in the spacing of cobalt and iron thin films on silicon oxide as a function of increasing film thickness and showed that the sign and magnitude of the thermal gradient can cause the size and spacing length scales to change. This mechanism does not appear to be operative in the liquid Cu−Si rings considered here because the film thickness for all of the rings is the same and the simulated thermal gradient in copper on silicon is only ~0.11 K/nm. This deviation from the R-P mechanism is also different than the one

reported by Favazza et al.,[30] where the prefactor in the ratio of the droplet distance and droplet size was found to differ (but remained constant) from the one expected on the basis of the R-P prediction. Our finding is that in the system considered here the scaling itself is modified, as discussed in more detail in what follows.

To understand the change in droplet spacing and the apparent instability mechanism in the copper rings, we consider the relevant timescales. Figure 4b shows the timescale associated with the cumulative transport (edge retraction), t_{ret}, combined with the timescale associated with R-P instability, $\tau_{m,riv}$, defined as $1/\sigma_{m,riv}$ (eq 6). For rings narrower than 200 nm, the retraction time is $t_{ret} < 7$ ns and $\tau_{m,riv} < 30$ ns, so the total transport plus instability time is less than the calculated time for the thin film instability to grow, which for 13 nm film is $\tau_{m,tf} = 1/\sigma_{m,tf} \approx 44$ ns. According to Figure 4b, the crossover point when $t_{ret} + \tau_{m,riv} \approx \tau_{m,tf}$ is reached for ring widths of $w \approx 260$ nm. This value is in reasonable agreement with the experimental ring width, $w \approx 215$ nm, at which the trend in the spacing between resulting nanoparticles changes. We note in passing that the timescales considered here are shorter than the liquid lifetime resulting from a single pulse. This observation, although consistent with the fully developed instability shown in Figure 1, a posteriori justifies the use of the original metal mass in our calculation because only a small percentage of metal mass is lost during a single pulse.

To conclude, it appears that for narrow rings the instability process is dominated by the R-P type of instability. However, for wider rings the cumulative timescale associated with the formation of a strip and the growth of the R-P instability is larger than the spinodal instability timescale, suggesting that thin film breakup is relevant here, leading to shorter wavelengths. We note here that the contraction of initial flat ring to a strip is so fast for all considered ring widths that thin film type of instability (either spinodal or nucleation) does not have time to grow to the point of breaking up a ring in the radial direction; however, the perturbation of the strip shape forms because the growth of a thin film instability is strong enough to lead to strip breakup on a length scale close to $\lambda_{m,tf}$.

To test this hypothesis further, we synthesized another set of copper rings of internal radius 5 and 10 μm with variable widths, this time with a thickness of $h_0 = 7$ nm. The reduced copper thickness modifies the relevant time and length scales, and the question is whether the theoretical setup discussed in the context of 13 nm thick films can be used to explain the experimental observations for 7 nm films.

Figure 5 shows scanning electron micrographs of a quarter of the rings as a function of ring width. We find an interesting trend in the nanodrop distribution as a function of the ring width, w: when w reaches 330 nm, the breakup changes from one-dimensional (in azimuthal direction only) to two-dimensional (azimuthal and radial). For the $w = 428$ nm rings, the initial ring appears to first break into two concentric rings which consequently break into nanoparticles. Figure 5b shows high resolution and tilted views (54°) of three 500 nm (inner) radius rings of variable widths that illustrate these three regimes. We note, perhaps surprisingly, that the instability develops faster for wider rings - e.g., in Figure 5b we already see clear formation of nanodrops for the 386 nm wide ring, while the 235 nm wide one is still evolving, and the breakup process has not been completed yet. Also of note, but beyond the discussion of this study, is the periodic secondary droplets that form at the inner and outer rims.

Figure 6 shows one-dimensional simulations analogous to the ones shown in Figure 3, for $h_0 = 7$ nm. This figure already shines some light into the experimental results shown in Figure 6. If a ring is wide enough, the thin film instability, which develops due

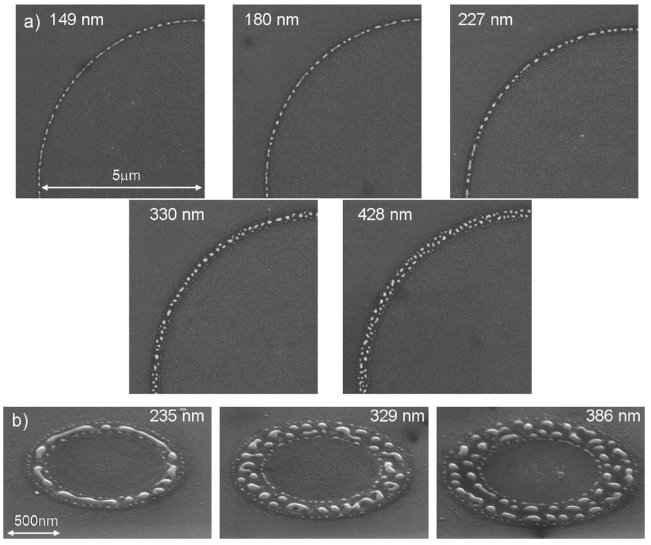

Figure 5. a) Scanning electron micrographs of the 7 nm thick, 5 μm radius copper rings with variable ring width after exposure to 2 laser pulses. b) Tilted (54°) images of three 500 nm radius rings with variable ring width demonstrating a change from azimuthal to azimuthal/radial breakup.

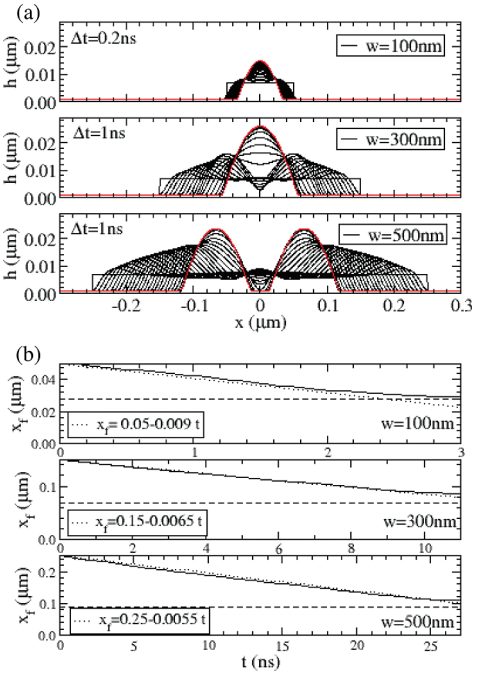

Figure 6. One dimensional time-dependent simulations of the $h_0 = 7$ nm thick copper ring cross section for 100, 300, and 500 nm wide rings (ignoring azimuthal curvature). a) Temporal profile of the film/strip height of the 100, 300, and 500 nm wide rings, demonstrating the timescale for formation of a semicylinder for each ring width. b) Edge (front) position, x_f, as a function of time. Solid line follows from simulations, and dotted line is a linear fit as shown.

to the presence of fronts, has sufficient time and space to grow while the film is contracting. This instability leads to the ring breakup in this one-dimensional geometry, considered extensively in earlier work.[8] Figure 6b shows numerically computed position of the front, together with the linear fit. These results, combined with the LSA, allow us to extract relevant time scales, which we discuss next.

Figure 7 shows the resultant length and timescale plots for the numerically calculated retraction, R-P, and spinodal instabilities

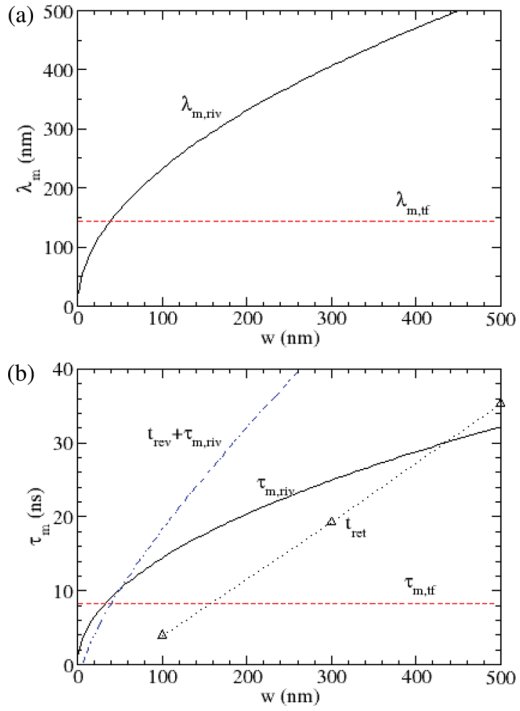

Figure 7. Length scale and timescale from linear stability analysis (LSA) and simulations (num.) for h_0 = 7-nm-thick copper strips as a function of the width, w. (a) Wavelength of maximum growth rate, λ_m, for the Rayleigh−Plateau (−) and thin film (spinodal) (---) instabilities. (b) Inverse of the maximum growth rate, τ_m, for the Rayleigh−Plateau (−) and thin film (spinodal) (---) instabilities. The symbols (△) represent numerically calculated retraction times, t_{ret}, obtained from Figure 6b. All calculations are based on the calculated Hamaker coefficient and the material properties in Table 1.

of the h_0 = 7 *nm* rings. We do not show experimental data here due to large scatter and the fact that the two-dimensional breakup changes the significance of the distance between droplets. In this figure, we see that for smaller w's (up to 200 nm or so), the relevant time scales are comparable, and it is not clear based on the comparison of time scales alone which instability mechanism is relevant. The experimental observation is that the average distance between the nanoparticles is slightly larger than 200 nm, which is again inconclusive.

However, for wider rings, Figure 7b shows that $\tau_{m,tf}$ becomes by far the shortest timescale in the problem, suggesting that radial instability is relevant. Further inspection of Figure 7b shows that the most unstable wavelength, $\lambda_{m,tf} \approx 150$ nm $< w/2$, and therefore for widths larger than 300 nm or so, the radial breakup of a ring may occur, as already suggested by Figure 6. These results now provide a good qualitative description of the experimental results shown in Figure 5. We note that the shortness of $\tau_{m,tf}$ can also be used to understand fast instability development for wide rings.

The proposed instability mechanism is then that for wider rings the thin-film instability, influenced also by the presence of fronts/edges, leads to the breakup of a ring in the radial direction into two concentric rings. These rings then break up into nanodrops according to the R-P mechanism. Because of the breakup in the radial direction, the distance between the nanodrops resulting from the R-P instability is not as large as may be expected from Figure 7a because the relevant widths are just half (or smaller) of the original ring width. Therefore, the expected distance between the nanodrops is in the range of 200−300 nm (Figure 6a), consistent with the experimental results shown in Figure 5.

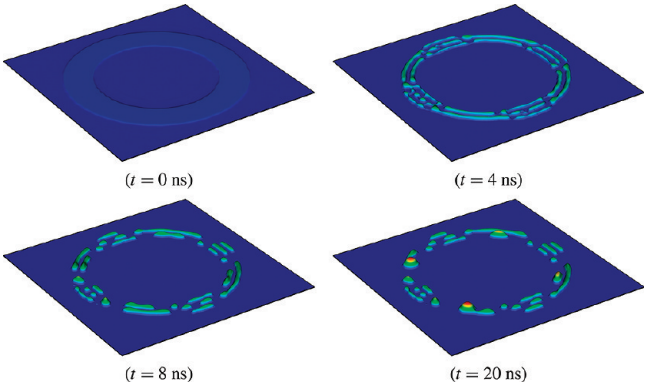

Figure 8. Time-dependent nonlinear simulations of an h_0 = 7-nm-thick ring with an inner radius of 1000 nm and a width of 500 nm. The initial shape is perturbed by random perturbations that are not visible on the scale shown.

Finally, to illustrate the instability development further, in Figure 8 we show an example of fully nonlinear simulations of ring geometry using the computational methods developed earlier and implemented for a number of related problems; see ref 21 and the references therein. Here we perturb the initial ring by random perturbations of small amplitude and observe their evolution. One can clearly observe the breakup mechanisms discussed above, on the correct timescales. One can also observe the significant distribution of particles sizes and distances, as in experiments. A detailed computational study of this problem, including the effects of azimuthal curvature, will be the subject of future work.

Conclusions

We have studied experimentally, computationally, and theoretically the pulsed-laser-heated assembly of lithographically patterned copper rings into organized nanodrops/particles. Theoretical and computational work required the Hamaker constant as a parameter. This quantity was determined by carrying out additional experiments involving the dewetting of continuous thin films and carrying out linear stability analysis, which allowed us to extract the Hamaker constant based on the length scales emerging during dewetting. This procedure has allowed us to carry out the theoretical analysis of ring breakup without any adjustable parameters. For 13-nm-thick copper rings, the nanoparticle length scale that emerges is a function of competing transport and instability mechanisms. We propose that the discontinuity observed in the dependence of nanodrop spacing on ring width is due to a shift from a Rayleigh−Plateau instability for narrow rings to a thin film instability for wider rings. The transition is ascribed to the cumulative time for the semicircular strip formation and Rayleigh−Plateau instability, which for rings of widths w > 265 nm is longer than the calculated thin film spinodal instability timescale. For thinner (7 nm) rings, assuming that the spinodal instability of a thin film is a relevant instability mechanism, we find that this instability is fast enough that for wider films it has sufficient time to lead to the breakup of the original ring into two concentric rings, which then consequently break up into nanoparticles following the Rayleigh−Plateau mechanism. We leave the details of the discussion of the thin film instability mechanism to future work.

This work demonstrates the interesting correlation that transport and instability timescales have on the resultant length scales, which is of critical importance in self-assembly and directed

assembly. In addition, we find it encouraging that good agreement among simulations, analysis, and computations is found, suggesting the significant utility of relatively simple modes in understanding instabilities on the nanoscale.

Acknowledgment. P.D.R. and J.D.F. acknowledge support from the Material Sciences and Engineering Division Program of the DOE Office of Science (ERKCM38). L.K. acknowledges that a portion of this research was conducted at the Center for Nanophase Materials Sciences, which is sponsored at Oak Ridge National Laboratory by the Division of Scientific User Facilities, U.S. Department of Energy, and partial support by NSF grant no. DMS-0908158. J.A.D. acknowledges support from Consejo Nacional de Investigaciones Científicas y Técnicas de la República Argentina (CONICET) and from Agencia Nacional de Promoción Científica y Tecnológica (ANPCyT) through grant PICT 2498/06.